ACCOUNTS
of chemical research

Impact Excitation and Electron–Hole Multiplication in Graphene and Carbon Nanotubes

NATHANIEL M. GABOR

Department of Physics, Massachusetts Institute of Technology, Cambridge, Massachusetts 02139, United States

RECEIVED ON JUNE 28, 2012

CONSPECTUS

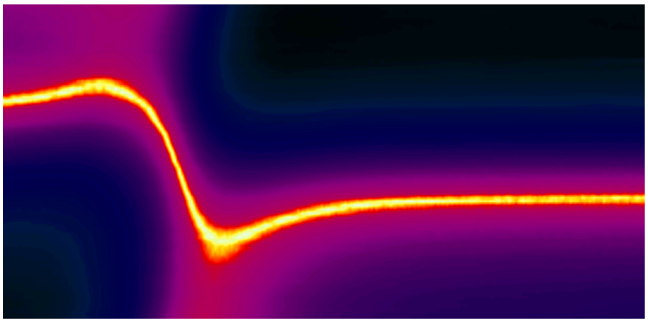

In semiconductor photovoltaics, photoconversion efficiency is governed by a simple competition: the incident photon energy is either transferred to the crystal lattice (heat) or transferred to electrons. In conventional materials, energy loss to the lattice is more efficient than energy transferred to electrons, thus limiting the power conversion efficiency. Quantum electronic systems, such as quantum dots, nanowires, and two-dimensional electronic membranes, promise to tip the balance in this competition by simultaneously limiting energy transfer to the lattice and enhancing energy transfer to electrons. By exploring the optical, thermal, and electronic properties of quantum materials, we may perhaps find an ideal optoelectronic material that provides low cost fabrication, facile systems integration, and a means to surpass the standard limit for photoconversion efficiency.

Nanoscale carbon materials, such as graphene and carbon nanotubes, provide ideal experimental quantum systems in which to explore optoelectronic behavior for applications in solar energy harvesting. Within essentially the same material, researchers can achieve a broad spectrum of energetic configurations, from a gapless semimetal to a large band-gap semiconducting nanowire. Owing to their nanoscale dimensions, graphene and carbon nanotubes exhibit electronic and optical properties that reflect strong electron–electron interactions. Such strong interactions may lead to exotic low-energy electron transport behavior and high-energy electron scattering processes such as impact excitation and the inverse process of Auger recombination. High-energy processes, which become very important under photoexcitation, may be particularly efficient in nanoscale carbon materials due to the relativistic-like, charged particle band structure and sensitivity to the dielectric environment. In addition, due to the covalently bonded carbon framework that makes up these materials, electron–phonon coupling is very weak. In carbon nanomaterials, strong electron–electron interactions combined with weak electron–phonon interactions results in excellent optical, thermal and electronic properties, the exploration of which promises to reveal fundamentally new physical processes and deliver advanced nanotechnologies.

In this Account, we review the results of novel optoelectronic experiments that explore the intrinsic photoresponse of carbon nanomaterials integrated into nanoscale devices. By fabricating gate voltage-controlled photodetectors composed of atomically thin sheets of graphene and individual carbon nanotubes, we are able to fully explore electron transport in these systems under optical illumination. We find that strong electron–electron interactions play a key role in the intrinsic photoresponse of both materials, as evidenced by hot carrier transport in graphene and highly efficient multiple electron-hole pair generation in nanotubes. In both of these quantum systems, photoexcitation leads to high-energy electron–hole pairs that relax energy predominantly into the electronic system, rather than heating the lattice. Due to highly efficient energy transfer from photons into electrons, graphene and carbon nanotubes may be ideal materials for solar energy harvesting devices with efficiencies that could exceed the Shockley–Queisser limit.

Published on the Web 01/31/2013 www.pubs.acs.org/accounts
10.1021/ar300189j

Introduction

Quantum optoelectronic materials, in which the optical and electronic properties directly reflect the quantum nature of electrons, promise to provide evolutionary and revolutionary advances in solar energy harvesting technologies. Numerous materials, including semiconductor quantum dots,[1−3] nanowires,[4,5] and nanotubes,[6,7] as well as organic and inorganic molecules,[8,9] are being actively explored for their potential in low-cost synthesis, fabrication, and system integration. While important for practical applications, quantum materials provide a playground for the exploration of fundamentally new energy conversion and energy relaxation processes, such as impact excitation (IE) and multiple electron–hole (e–h) pair generation. These processes, which could improve the efficiency of photovoltaic cells beyond standard thermodynamic limits,[10] have been the subject of intense multidisciplinary research and have caught the interest of chemists, materials scientists, engineers, and physicists.

By comparing the incident photon energy, E_{PH}, to the band gap energy, E_{GAP}, we can describe three important photoelectronic energy regimes that can be explored in quantum materials (Figure 1). The first regime (Figure 1A), in which the ratio $E_{PH}/E_{GAP} \approx 1$, is the regime in which power conversion approaches the thermodynamic (Shockley–Queisser) limit.[10] As the ratio increases to $E_{PH}/E_{GAP} > 2$, electron–electron interactions may lead to multiple e–h pair generation, increasing the efficiency beyond the standard limit. The third, and perhaps least explored, regime is that in which E_{GAP} approaches zero, or $E_{PH}/E_{GAP} \rightarrow \infty$ (Figure 1C). In this regime, strong electron–electron interactions may drive hot carrier effects that allow yet higher energy conversion efficiency.[11]

Carbon-based nanomaterials, such as monolayer graphene (MLG) and nanotubes (NTs), allow us to explore the full spectrum of photoelectronic energy regimes. The enthusiasm surrounding the optical and electronic properties of these materials arises from the peculiar band structure of graphene.[12−15] Graphene, which is a two-dimensional array of carbon atoms arranged in a honeycomb lattice (Figure 2A), exhibits zero band gap energy. Over a broad range of energies (approximately ±1eV), the electron–hole symmetric bands $\varepsilon(k)$ (Figure 2B) are approximately conical and result in charge carriers with the same Fermi velocity, $v_F \approx 10^6$ m/s. In contrast to both metals and semiconductors, at low energies, the conduction and valence band touch (at the so-called charge neutrality point). Here, the electronic density of states $g(\varepsilon)$ approaches zero, leading graphene to be characterized as a semimetal. Importantly, the electrons in MLG behave as a gas of massless Dirac fermions, that is, they are described by the Dirac equation for massless particles, rather than the Shrödinger equation.[16]

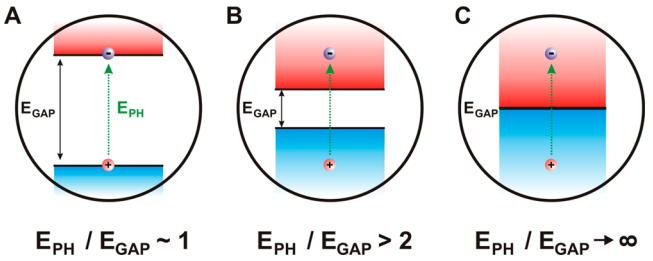

FIGURE 1. Schematic diagrams of the photoelectronic energy regimes in quantum materials including systems in which (A) E_{GAP} and E_{PH} are comparable, (B) E_{PH} is more than twice E_{GAP}, and (C) E_{PH} is very large compared with E_{GAP}.

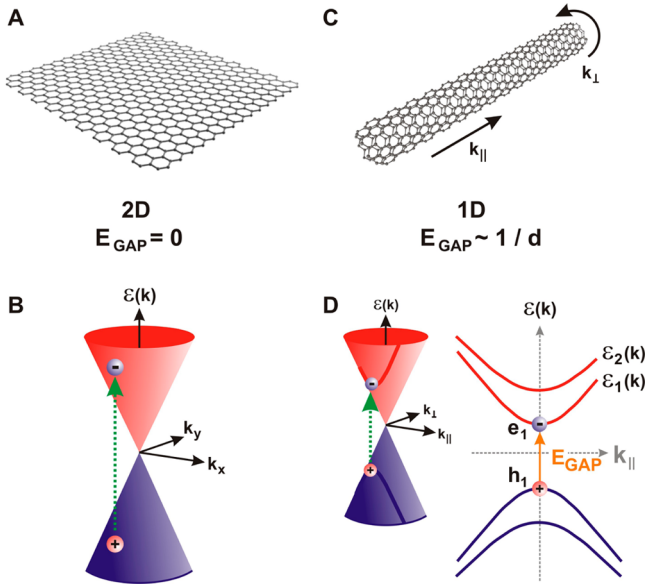

FIGURE 2. (A) Graphene, a single atom-thick sheet of hexagonally oriented carbon, and (B) its conical band structure in two dimensions. $\varepsilon(k)$ is the electron energy as a function of momentum in two dimensions, k_x and k_y. (C) A carbon nanotube formed by rolling the graphene sheet, and (D) its hyperbolic band structure in one dimension. The electron momentum perpendicular to the tube axis, $k_\perp$, is quantized resulting in a band gap, E_{GAP}.

Rolling graphene into a tube imposes boundary conditions on the electronic wave function, resulting in a one-dimensional nanowire with diameter-dependent band gap energies.[17−20] Along the circumference of the tube, the crystal momentum becomes quantized since the wave function must match itself as it completes one full circulation (Figure 2C). For a tube of diameter d, this gives the geometric condition $\Delta k_\perp \pi d = 2\pi$, where $k_\perp$ is the crystal momentum perpendicular to the tube axis. This quantization cuts a set of

discrete planes, $\varepsilon_1(k_\parallel)$, $\varepsilon_2(k_\parallel)$, ..., out of the Dirac cone with a spacing defined by the above expression. The intersection of planes (at intervals of $\Delta k_\perp$) with the allowed energies of the Dirac cone forms the one-dimensional subbands of NTs (Figure 2D), each with a van Hove singularity in the density of states ($g(\varepsilon) \rightarrow \infty$).

In low-dimensional materials, electron confinement and reduced electronic screening lead to drastically increased electron–electron (Coulomb) interactions. To compare the energy scale of Coulomb interactions to a scale relevant in carbon nanomaterials, it is interesting to note that the conical bands of graphene are light-like while the hyperbolic bands in NTs are analogous to the allowed energies of relativistic particles with relativistic energies mv_F^2. In relativistic particle physics, the occurrence of charged particle interactions depends strongly on the ratio of the Coulomb interaction strength between electrons to their relativistic energies and is quantified by the fine structure constant $\alpha = e^2/(4\pi\varepsilon_0\hbar c) \approx 1/137$, where ε_0 is the permittivity of vacuum. Interestingly, the Fermi velocity and low dielectric constant in MLG and NTs leads to an effective fine structure constant $\alpha = e^2/(4\pi\varepsilon\hbar v_F) \approx 1$, suggesting that electron–hole generation and annihilation should be quite efficient.

Within essentially the same hexagonal carbon material, a continuous spectrum of band gap energies can be achieved, thus allowing a direct probe of interacting electrons. The electronic properties that result are directly manifested in diverse aspects of MLG and NT photoresponse, which has been the focus of extensive research for optoelectronic and energy-harvesting applications. Here, we discuss optoelectronic measurements that explore the intrinsic photoresponse in carbon nanomaterials. As will be seen, our measurements demonstrate some of the unique properties of these materials but also reveal very unconventional behavior.

Optoelectronics in Carbon Nanomaterials

As physicists and nanotechnologists, our experimental approach takes inspiration from the compilation of knowledge based on over half a century of semiconductor technology. We aim to integrate MLG and NTs as the active element in photoconducting devices and study the optoelectronic characteristics. Before understanding the device behavior observed in MLG and NTs, however, it is important to understand the basic working principles of a conventional semiconductor optoelectronic device: the PN junction.

R. S. Ohl patented the first PN junction in 1941 while at Bell Telephone Laboratories.[21] Ohl's "light sensitive electric device" combines two semiconductor silicon crystals, one doped with electron donors (p-type material) and the other with electron acceptors (n-type material).[21,22] By placing the two materials together, Ohl discovered that charge at the interface is redistributed to form a built-in electric field. Because the PN junction is composed of semiconducting materials, the minimum energy required to excite an electron from the valence band to the conduction band is E_{GAP}. The resulting electronic potential energy and schematic device characteristics are shown in Figure 3A,B. In the absence of light, when a positive voltage is applied across the device, the potential energy barrier at the PN junction is reduced, resulting in exponential turn-on in forward bias. When a negative voltage is applied the potential barrier is increased, and no current passes through the device.

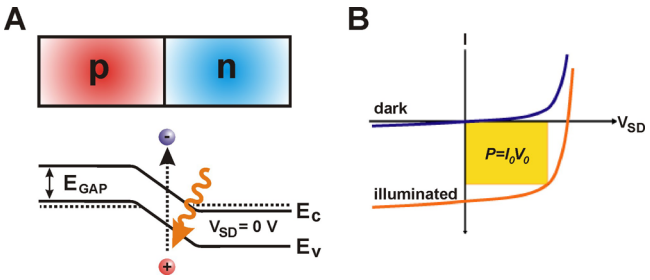

FIGURE 3. (A) Electronic potential energy landscape for a semiconductor PN junction at a source drain bias $V_{SD} = 0$. E_C and E_V are the conduction and valence band edges, respectively. (B) Conventional characteristics of a PN junction device in the dark and under illumination. Peak energy conversion efficiency occurs within the lower right quadrant.

If a photon whose energy exceeds E_{GAP} is incident on the PN junction, it creates an e–h pair that is separated by the electric field and collected at the contacts. This leads to additional current that offsets the dark I–V characteristic. In forward bias, the amount of optical power converted to electrical power generated in the device, $P = I_0V_0$, is the power conversion efficiency (Figure 3B). This is the basic operating regime of solar cell devices used for energy harvesting. In reverse bias, the built-in field may become so strong that carriers are accelerated to high kinetic energies and undergo avalanche multiplication. This is the operating regime of avalanche photodiodes. As we will discuss, quantum materials allow us to operate a PN junction that exhibits avalanche-like behavior in the forward bias power conversion regime, thus increasing the energy-harvesting efficiency.

To probe photoresponse in carbon nanomaterials, we fabricated and measured light-sensitive devices. Our PN junction devices consist of individual exfoliated MLG flakes or

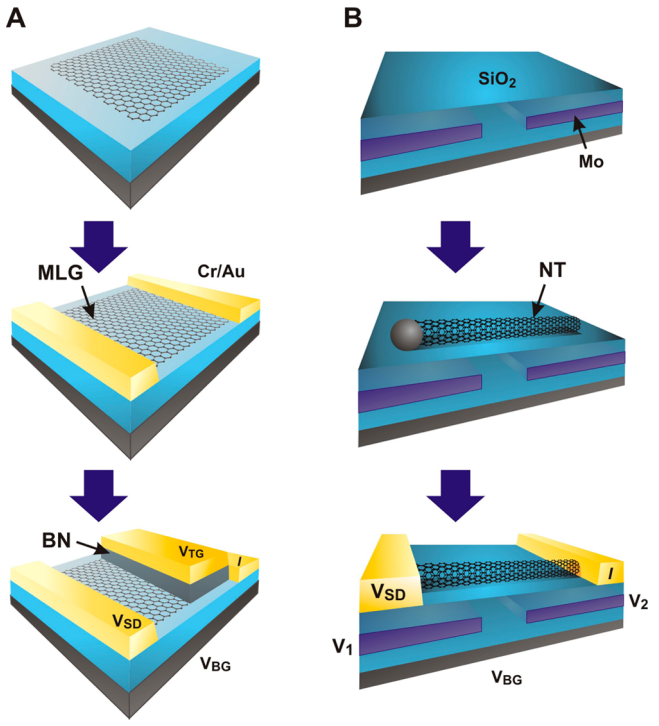

FIGURE 4. (A) Process flow for fabrication of the graphene multigate PN junction photodetector (discussed in text). Monolayer graphene (MLG) is the active material in a device integrated with hexagonal boron nitride (BN) insulator. (B) Process flow for the carbon nanotube (NT) split-gate photodiode. NTs are synthesized directly onto the device using chemical vapor deposition.

semiconducting NTs integrated into multigate geometries that allow local electrostatic doping.[23−27] Applying a voltage to a conducting gate electrode maintains a static charge distribution on the nearby MLG or NT. Through tuning of the gate voltage, the MLG flake or NT can exhibit ambipolar behavior: negative gate voltage leads to p-type conduction, while positive voltage results in n-type conduction. Fabricating multiple gates and exfoliating MLG or synthesizing NTs on the top surface of the device allows us to introduce various experimental probes (such as focused laser light) to the device channel.

Graphene PN junctions (Figure 4A) were fabricated by exfoliating high-quality graphene onto standard silicon substrates.[28] Thin gold electrodes were deposited to form electrical contacts to the graphene flakes. For the top-gate electrode of the PN junction device, we first mechanically exfoliated and then transferred boron nitride flakes over the entire device. Hexagonal boron nitride acts as an insulating layer over which a thin gold top-gate electrode was deposited using e-beam lithography and thermal evaporation.

For nanotube devices (Figure 4B), NTs were grown on a predefined split-gate substrate using the flying catalyst chemical vapor deposition (CVD) growth process.[24,29] The resultant NTs have lengths up to 10 μm and a diameter distribution centered at 1.5 nm with a range extending from 1 to 4 nm. After fabricating gold electrodes, we then probed electrical conductivity of the device junctions to identify those containing one or more NTs and measured the NT diameters using atomic force microscopy.

Although electronic and optical experiments give complementary insight into intrinsic photoresponse, it is extremely important to understand the interplay of optical and electronic behavior. The scanning photocurrent spectroscopy microscope (SPSM)[30] combines electronics and optics to investigate this interplay. In the SPSM, nanoscale devices are wired into an optical cryostat. Electronic feed-throughs allow the measurement of electronic properties while the device is illuminated at various temperatures. To generate a photocurrent image, a diffraction-limited beam spot is scanned over the device while the current is recorded. Simultaneously, reflected light from the sample is collected, and the reflected intensity is monitored to form a correlated image of the device. Using this technique, we are able to probe the interplay of optical excitations and electronic transport in MLG and NTs.

Hot Charge Carriers and Impact Excitation in Graphene

The photoconversion efficiency of semiconductors is governed by the competition between various energy relaxation pathways of photoexcited e–h pairs: energy transferred to the lattice is converted to heat, while energy transported through charge carriers may be used to drive an optoelectronic circuit.[22] In graphene, energy relaxation pathways are strongly altered by the vanishing electronic density of states near the charge neutrality point.[31−33] High-energy e–h pairs may relax by colliding with, creating, or annihilating other fundamental quasi-particles. One class of quasi-particles, optical phonons, has been well studied[34] and are known to interact strongly with high-energy carriers in MLG. However, after initial relaxation of photoexcited carriers caused by electron–electron scattering and optical phonon emission, electron–lattice energy relaxation can be quenched due to very weak acoustic phonon scattering.[31] Weak phonon scattering combined with vanishing density of states creates a bottleneck that limits further energy redistribution into the lattice. With electron-to-lattice energy relaxation quenched, a novel transport regime is reached in which thermal energy is redistributed solely among electronic charge carriers. Electrons and holes remain hot while the lattice stays cool.

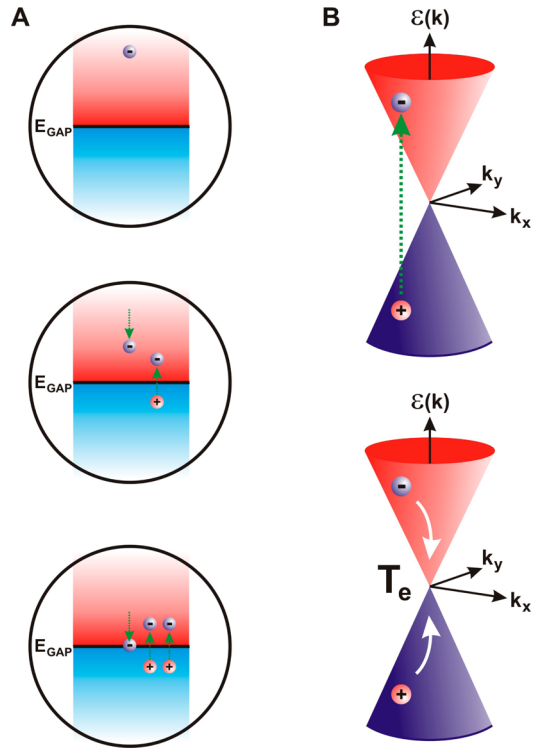

FIGURE 5. (A) Impact excitation in a zero band gap system, such as graphene. The initial electron may relax to excite several e–h pairs of lower kinetic energy, creating a distribution of hot carriers. (B) Photon absorption in graphene's conical bands leads to a high-energy electron and hole that subsequently relax to form a hot temperature distribution with an electronic temperature, T_e. Image taken from ref 30.

In graphene, optically excited electrons and holes have been predicted to undergo IE, a process by which high-energy carriers collide with or generate low-energy carriers.[32,35,36] By comparing electron and phonon heat capacities, Song et al.[33] suggested that electron–electron interactions dominate thermal energy transfer from the initial photoexcitation into graphene's electronic and phonon subsystems. The primary electron scattering process that redistributes energy within the electronic system is impact excitation. To reach the hot carrier regime, IE competes with Auger recombination to establish an equilibrium electronic temperature T_e. In the absence of a band gap, a high-energy charge carrier may relax through several collisions to produce multiple e–h pairs (Figure 5A). In the simplest view, since the activation energy for a new e–h pair is infinitesimal, IE may occur with very high quantum efficiency leading to avalanche-like behavior. However, the available electronic states decrease as electrons and holes fill states near the charge neutrality point. Near the charge neutrality point, where the density of states $g(\varepsilon)$ is very small and approaches zero, the increase of the electronic temperature dT_e can be determined thermodynamically (Figure 5B):

$$dT_e = \frac{dQ_e}{C_e} \approx \frac{dQ_e}{g(\varepsilon)} \quad (1)$$

where dQ_e is the energy provided to the electronic system by photons, and $C_e \propto g(\varepsilon)$ is the heat capacity of the electronic system. As the density of states, $g(\varepsilon)$, approaches zero, eq 1 implies that competition between IE and Auger annihilation results in a very hot electron–hole population. Experimentally, a hot electronic temperature near the charge neutrality point may serve as evidence of electron–electron interactions.

Due to very weak acoustic phonon emission, hot electrons in MLG were predicted[31,33] and observed[37] to exhibit very long cooling times that exceed hundreds of picoseconds. After optical frequency excitation, optical phonon emission and electron–electron scattering dominate electronic relaxation on very short time scales (within ~1 ps).[37] Once carrier energies are reduced to below the optical phonon energy ($\hbar\omega \approx 0.2$ eV), weak acoustic phonon emission is the primary energy relaxation channel. Song et al.[33] proposed that hot carrier transport effects in MLG, such as the photothermoelectric effect (first observed by Xu et al.[38]) and long cooling times, might signal the presence of highly efficient carrier scattering. Additionally, simulations[32] have shown that IE may dominate over Auger recombination, resulting in high-efficiency carrier multiplication. Most importantly for optoelectronics, long-lived photoexcited carriers in graphene may remain in an excited state long enough to be efficiently harvested and drive a photothermoelectric effect in a graphene device.

Recently, we used scanning photocurrent microscopy to demonstrate that hot carriers indeed play a key role in the photoresponse of graphene.[28] We studied multigated PN junctions both in monolayer (MLG) and bilayer graphene. Tuning the bottom and top gate voltages, V_{BG} and V_{TG}, respectively, allowed independent control of carrier density and polarity (n-type or p-type) in each region. Resistance characteristics, R vs V_{BG} and V_{TG}, exhibit two intersecting lines of relatively high resistance and a maximum resistance, R_{max}, at their intersection, the global charge neutrality point (Figure 6B). These two lines divided the resistance map into four regions: p–n, n–n, n–p, and p–p, labeled according to the carrier doping induced in the bottom-gated and dual-gated regions (regions 1 and 2, respectively).

We established a PN junction by applying voltages of opposite polarity on V_{BG} and V_{TG}. Figure 6C shows a photocurrent image of the PN junction at an excitation wavelength

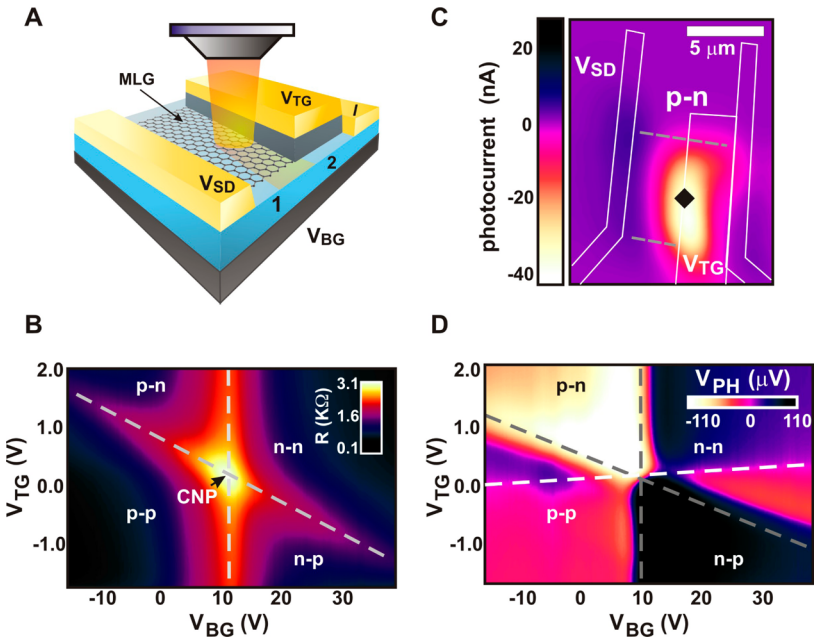

FIGURE 6. (A) The graphene PN junction under focused laser illumination in the scanning photocurrent spectroscopy microscope. Region 1 is covered only by the ultrathin BN while region 2 has an additional top-gate electrode. (B) Resistance across the graphene channel vs top-gate, V_{TG}, and bottom-gate, V_{BG}, voltages. A high resistance peak occurs when the electron density is tuned to zero in both regions, called the charge neutrality point. (C) A scanning photocurrent image exhibits a strong response at the location of the interface between p-type and n-type regions. (D) Photovoltage V_{PH} vs gate voltages (same as in panel B). Whereas the resistance only shows four regions, the photovoltage exhibits six regions, characteristic of the photothermoelectric effect. Image adapted from ref 28.

of $\lambda = 850$ nm. Optoelectronic measurements with the laser fixed at the p–n interface exhibited a striking photovoltage pattern with six regions of alternating photovoltage sign as a function of V_{BG} and V_{TG} (Figure 6D). The sign and magnitude of photovoltage depends on the Seebeck coefficient[38,39] in each region and can be written as

$$V_{PTE} = (S_2 - S_1)\Delta T \tag{2}$$

where S is thermoelectric power (Seebeck coefficient) in regions 1 and 2, and ΔT is proportional to the electron temperature difference between the area under the laser spot and its surroundings.[33] From the Mott formula,[39] we can write S as

$$S = \frac{\pi^2 k_B{}^2 T}{3e} \frac{1}{R} \frac{dR}{dV_G} \frac{dV_G}{dE}\bigg|_{E=E_F} \tag{3}$$

where T is the sample temperature, k_B is the Boltzmann constant, and E_F is the chemical potential.[38] The nonmonotonic dependence of S_1 and S_2 resulted in multiple sign reversals for the quantity $(S_1 - S_2)$, which gave rise to the 6-fold pattern (Figure 6D), characteristic of a photothermoelectric effect in graphene.[33]

Further experiments showed that graphene's photoresponse exhibits charge density dependence and long cooling lengths that support hot carrier-assisted transport of thermal energy. While our measurements provide direct evidence for hot carriers that proliferate throughout the system, they may also serve as indirect evidence of IE processes.

How can IE and multiple e–h pair generation be verified in graphene? Recent calculations by Winzer and Malic[32,36] have focused on the subpicosecond dynamics of charge carriers and suggest that time-resolved photoresponse measurements may provide evidence for multiple e–h pair generation and Auger annihilation. A more direct approach of probing multiplication may lie in devices similar to energy-resolving superconductor photodetectors.[40] In these devices, high-energy photons (~1 eV) are used to break apart low-energy Cooper pairs (~1 meV), resulting in a voltage build-up across a superconducting junction. The number of broken Cooper pairs, and therefore the voltage response, increases with photon energy. Similarly, increase in MLG's photoresponse as a function of photon energy may be a direct experimental indicator of efficient IE.

Multiple Electron–Hole Pair Generation in Carbon Nanotubes

In conventional semiconductors, conduction band carriers can gain sufficient kinetic energy to collide with valence band carriers and generate an additional e–h pair via impact

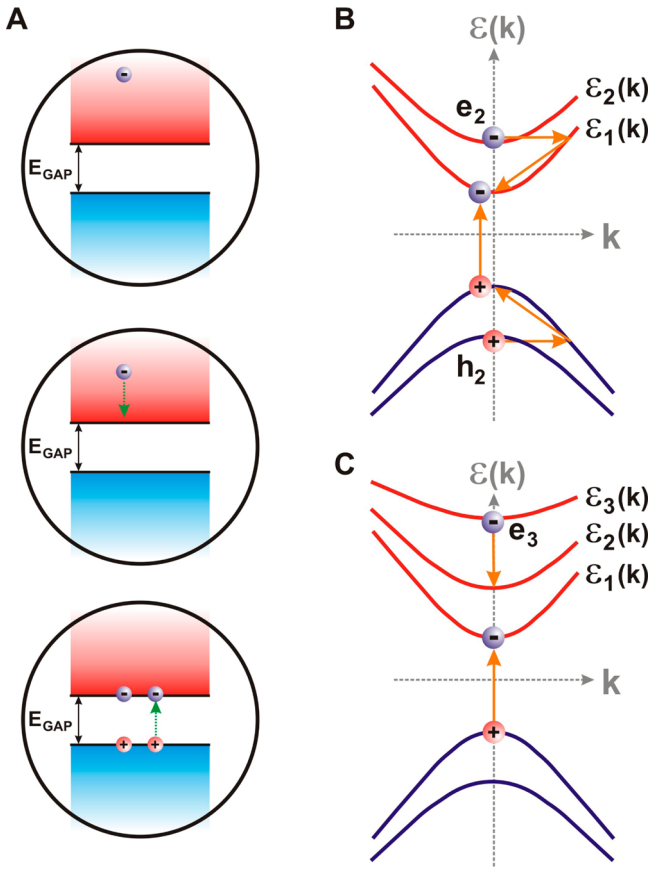

FIGURE 7. (A) Impact excitation in a gapped electronic system, such as semiconducting carbon nanotubes. The initial electron may relax to excite multiple e–h pairs of lower kinetic energy. The lowest energy IE processes in the NTs hyperbolic band structure occur via two-body (B) or three-body (C) interactions, as discussed in text. Image taken from ref 30.

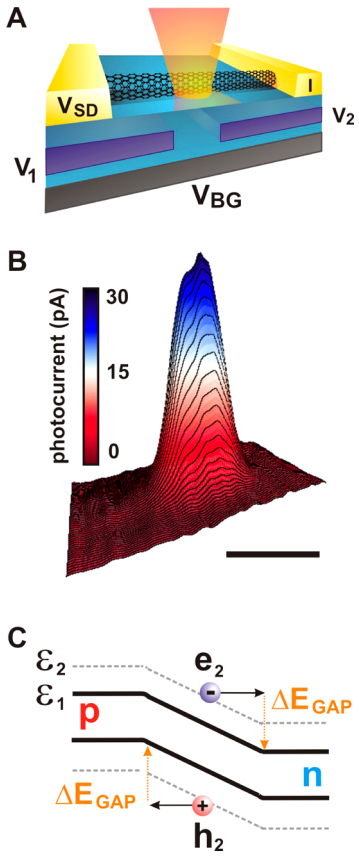

FIGURE 8. (A) The NT photodiode under focused laser illumination in the scanning photocurrent spectroscopy microscope. (B) A scanning photocurrent image exhibits a strong photoresponse at the location of the interface between p-type and n-type regions. (C) A schematic diagram of the IE process in one dimension. High-energy electrons and holes (with energies greater than $2E_{GAP}$) combine E_{PH} and the energy provided by the electric field to undergo IE, leading to multiple electron–hole pair generation. Image adapted from ref 29.

ionization.[22] This process, shown in Figure 7A, converts excess kinetic energy into additional charge. In NTs, interactions between higher subband electrons and holes become important, and one-dimensional momentum conservation must be considered. Here, we describe the two lowest energy e–h pair generation processes that have been proposed in NTs: a two-body process by which a high-energy correlated e–h pair relaxes into two low-energy e–h pairs (proposed by Kane and Mele[41]) and a three-body interaction in which a highly energetic electron (or hole) relaxes to create a new electron and hole (Perebeinos et al.[42]).

In the NT single particle band structure, the second subband $E_{22} \approx 2E_{GAP}$ corresponds to excitations of more massive particles ($m_2^* = 2m_1^*$). As shown in Figure 7B, an e–h pair initially at the second subband edge can relax into an e–h pair in the first subband with a finite kinetic energy. Because $E_{22} \approx 2E_{GAP}$, this strongly interacting e–h pair has sufficient excess energy to relax into two e–h pairs via the process $e_2^2 + h_2^2 \rightarrow (e_1^1 + h_1^1) + (e_1^1 + h_1^1)$, where the subscripts indicate the subband index and the superscript is the transverse momentum of the carrier in units of $2/(3d)$. Kane and Mele[41] studied this process analytically and showed that it may occur with high efficiency in NTs. While this process is possible in the single particle band structure of NTs, strong Coulomb interaction effects renormalize the band structure such that $E_{22} < 2E_{11}$. Following their analysis, strongly bound e–h pair correlations (excitons) in NTs have been shown to dominate the optical response,[43] and additional theoretical work[44] has found that multiple excitons may be generated due to resonant coupling of one-exciton and two-exciton states.

By considering strict conservation of energy and momentum in the NT band structure, Perebeinos et al.[42] showed that carriers in the third subband may undergo IE via the process $e_3^4 \rightarrow e_2^2 + (e_1^1 + h_1^1)$, which occurs equivalently for holes. This process (shown in Figure 7C) converts an e_3 electron into an e_2 electron and an additional electron and

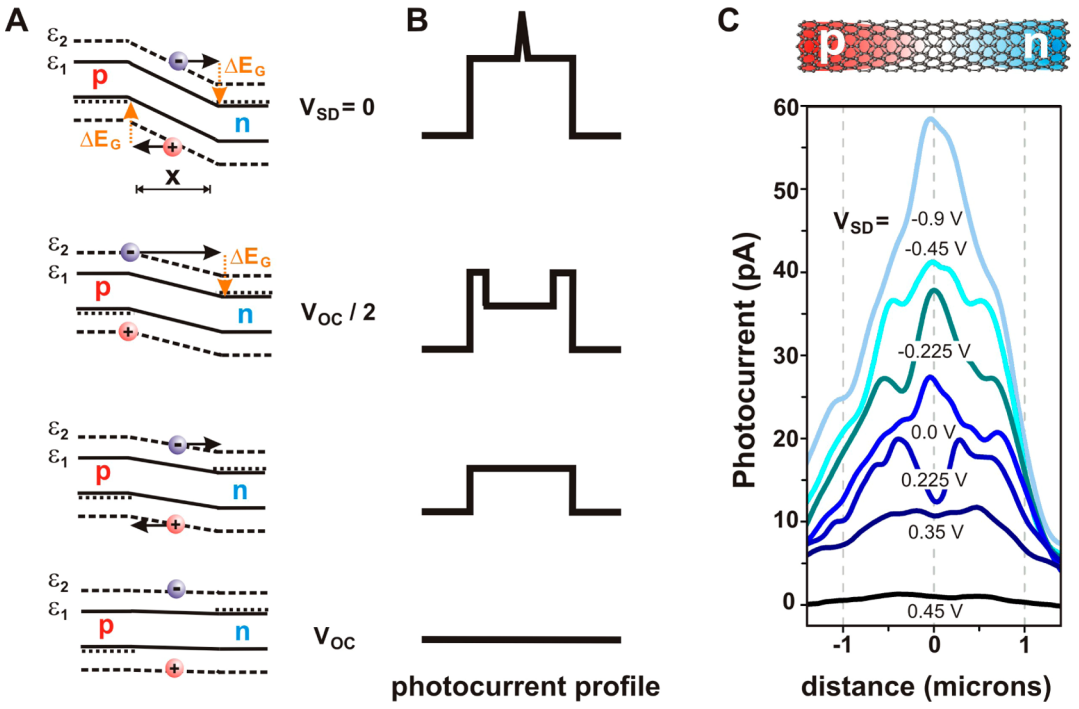

FIGURE 9. (A) Schematic diagrams of the IE process at various values of the source drain bias, V_{SD}, which controls the electric field strength across the PN junction. The electric field increases from bottom to top. (B) Expected linear photocurrent profile in the presence of IE due to high-energy electrons and holes at corresponding V_{SD} values. (C) Observed photocurrent profiles of the NT PN junction at relevant V_{SD} values. The lowest four traces show strong agreement with the expectations of IE. Image adapted from ref 29.

hole in the first subband. The transverse momentum of the e_3 electron $4 \times 2/(3d)$ is transferred to a second subband carrier (resulting in transverse momentum $2 \times 2/(3d)$) and two first subband carriers. While similar processes occur for higher subbands, this process is the lowest energy three-body creation process that conserves transverse momentum.

A powerful way to directly probe multiplication processes is through measuring the photoresponse of the nanotube PN junction using SPSM (Figure 8A). Figure 8B shows a photocurrent map taken with an excitation wavelength of $\lambda = 532$ nm. A photocurrent peak is observed at the PN junction, with a full width at half-maximum of ~700 nm perpendicular to the NT, consistent with the size of the excitation beam.

From detailed photocurrent spectroscopy measurements,[29,30] we attributed photocurrent enhancement above $E_{22} \approx 2E_{GAP}$ to efficient e–h pair generation by high-energy charge carriers in the second NT subband. In this process, the excess rest mass energy of the second subband carriers ($m_2^* v_F^2$) is combined with the kinetic energy of the electric field to create an e_1 carrier plus e–h pairs (Figure 8C),

$$e_2 + K_e(x) \rightarrow e_1 + n(e_1 + h_1) \quad (4a)$$

and, equivalently for holes,

$$h_2 + K_h(x) \rightarrow h_1 + n(e_1 + h_1) \quad (4b)$$

The integer $n = 1, 2, 3, \ldots$ indicates the number of pairs produced. As shown in Figure 9A, the kinetic energy available to electrons (K_e) and holes (K_h) created at a position x along the PN junction can be tuned by changing V_{SD}. At the open circuit voltage, $V_{SD} = V_{OC} \approx E_{GAP}/e$, the total potential energy drop is zero, resulting in a flat spatial photocurrent profile (Figure 9B, bottom). Conversely, at $V_{SD} = 0$, the total potential energy available along the entire junction is E_{GAP} (Figure 9B, top).

Our model suggests that energy gained by a carrier in the PN junction depends strongly on its initial location. As V_{SD} reaches the threshold $V_{SD} = {}^1/_2 V_{OC}$, a carrier excited at the edge of the junction, either the electron or the hole, picks up the entire potential energy of the junction and undergoes IE. At this voltage, the power conversion efficiency is strongly enhanced due to IE. At $V_{SD} = 0$, the electron and hole created at the center each pick up half of the junction's potential energy, leading to additional gain.

Spatial photocurrent measurements provide a detailed probe to confirm our impact excitation model. In Figure 9C, we plot photocurrent profiles for a device of $V_{OC} = 0.45$ V taken by scanning the laser along the length of the nanotube at various V_{SD} values. At $V_{SD} = 0.35$ V, the IE threshold is not reached, and we observed a flat photocurrent profile.

At $V_{SD} = V_{OC}/2 = 0.225$ V, the photocurrent profile exhibits double-peaked maxima occurring at the edges of the PN junction, corresponding to IE. When the bias voltage reaches $V_{SD} = 0$ V, an additional sharp increase occurs at the center of the device, corresponding to additional IE events. In reverse bias, the photocurrent peaks at the edges catch up to the center peak (at $V_{SD} = -V_{OC}$) until finally, at high reverse bias, the center peak again dominates over the side peaks.

Additional work continues to investigate the details of impact excitation in NTs. In contrast to Perebeinos et al.,[42] we observed IE in the second subband, suggesting that either other carriers or phonons are involved to conserve momentum. Baer et al.[45] reconciled the difference between our results and the theory of Perebeinos by proposing an important variation. In their model, the initial excitation above the second subband ε_2 relaxes very quickly into an ε_1 electron (hole) and an ε_3 hole (electron). Interactions of the ε_3 carriers with the electric field leads to the efficient IE process described by Perebeinos et al. More recently, ultrafast photoresponse techniques[46,47] that access real-time transit of electrons in NT devices have been developed to explore these interactions and perhaps unravel the details of the IE process.

Interestingly, earlier experiments on NTs attributed electroluminescence[48−50] and avalanche breakdown[51] to pair generation by IE. Additionally, transient absorption spectroscopy measurements on chemically isolated NTs were used to observe multiple exciton generation (MEG).[52,53] In these measurements, absorption of single photons with energies corresponding to $3E_{GAP}$ resulted in an efficiency of 130%. Consistent with our measurements, at photon energies above $2E_{GAP}$, Wang et al.[53] also observed an increase in MEG efficiency at room temperature. In order to understand the details of this process, further experiments that probe the number of multiplied carriers and their initial energies are needed.

Shining Light on the Future of Carbon Nanomaterials

By understanding impact excitation and multiple electron−hole pair generation, we may improve the efficiency of R. S. Ohl's "light sensitive device" to achieve solar power conversion beyond the limits set out by Shockley and Queisser. However, experiments that explore multiplication processes, particularly in carbon-based nanomaterials, only give a glimpse of the physical processes involved. In monolayer graphene, a direct observation of multiplication and annihilation processes is still lacking. In carbon nanotubes, the process has only been demonstrated, and further work will continue to explore the intricate details. As we have shown, multiplication processes indeed play an important role in this intrinsic photoresponse, yet many questions remain.

Just as the hydrogen atom serves as the gold standard for understanding quantized electronic systems, graphene may serve as the next-generation standard for understanding higher-dimensional quantum systems. Graphene and carbon nanotubes exhibit many unique properties, several of which have been highlighted here. However, these materials are only examples within a class of materials in which the electron dynamics are described by the Dirac equation. While it is clear that efficient impact excitation, particularly in MLG and NTs, may improve solar energy conversion, such processes may also give us deeper understanding of Dirac-like electron dynamics. To truly grasp the potential of these materials, we must understand the electron dynamics, as well as the resulting optical, thermal, and electronic properties. Although the quantum physics understood from atomic hydrogen continues to serve us well, perhaps it is time for atomically thin carbon to guide us into the future.

BIOGRAPHICAL INFORMATION

Nathaniel Gabor, currently working as a Research Fellow with Pablo Jarillo-Herrero in the Physics Department at the Massachusetts Institute of Technology, completed his Ph.D. in experimental physics under the supervision of Paul McEuen at Cornell University in 2010. Before attending Cornell, Nathaniel completed his undergraduate degree in Physics at the Pennsylvania State University. Nathaniel's research has focused on quantum optoelectronic measurements of nanoscale carbon materials including graphene and individual carbon nanotubes.

FOOTNOTES

The author declares no competing financial interest.

REFERENCES

1 Schaller, R.; Klimov, V. High Efficiency Carrier Multiplication in PbSe Nanocrystals: Implications for Solar Energy Conversion. *Phys. Rev. Lett.* **2004**, *92*, No. 186601.

2 Ellingson, R. J.; Beard, M. C.; Johnson, J. C.; Yu, P.; Micic, O. I.; Nozik, A. J.; Shabaev, A.; Efros, A. L. Highly Efficient Multiple Exciton Generation in Colloidal PbSe and PbS Quantum Dots. *Nano Lett.* **2005**, *5*, 865–861.

3 Gur, I.; Fromer, N. A.; Geier, M. L.; Alivisatos, A. P. Air-Stable All-Inorganic Nanocrystal Solar Cells Processed from Solution. *Science* **2005**, *310*, 462–465.

4 Li, Y.; Qian, F.; Xiang, J.; Lieber, C. M. Nanowire Electronic and Optoelectronic Devices. *Mater. Today.* **2006**, *9*, 18–27.

5 Garnett, E. C.; Brongersma, M. L.; Cui, Y.; McGehee, M. D. Nanowire Solar Cells. *Annu. Rev. Mater. Res.* **2011**, *41*, 269–295.

6 Wu, Z.; Chen, Z.; Du, X.; Logan, J. M.; Sippel, J.; Nikolou, M.; Kamaras, K.; Reynolds, J. R.; Tanner, D. B.; Hebard, A. F.; Rinzler, A. G. Transparent, Conductive Carbon Nanotube Films. *Science* **2004**, *305*, 1273–1276.

7 Avouris, P.; Freitag, M.; Perebeinos, V. Carbon Nanotube Photonics and Optoelectronics. *Nat. Photonics* **2008**, *2*, 341–350.

8 Hagfeldt, A.; Gratzel, M. Molecular Photovoltaics. *Acc. Chem. Res.* **2000**, *33*, 269–277.

9 Hardin, B. E.; Snaith, H. J.; McGehee, M. D. The Renaissance of Dye-Sensitized Solar Cells. *Nat. Photonics* **2012**, *6*, 162–169.

10 Shockley, W.; Queisser, H. J. Detailed Balance Limit of Efficiency of p-n Junction Solar Cells. *J. Appl. Phys.* **1961**, *32*, 510–519.

11 Ross, R. T.; Nozik, A. J. Efficiency of Hot-Carrier Solar Energy Converters. *J. Appl. Phys.* **1982**, *53*, 3813–3818.

12 Geim, A. K.; Novoselov, K. S. The Rise of Graphene. *Nat. Mater.* **2007**, *6*, 183–191.

13 Castro Neto, A. H.; Guinea, F.; Peres, N. M. R.; Novoselov, K. S.; Geim, A. K. The Electronic Properties of Graphene. *Rev. Mod. Phys.* **2009**, *81*, 109–162.

14 Avouris, P. Graphene: Electronic and Photonic Properties and Devices. *Nano Lett.* **2010**, *10*, 4285–4294.

15 Bonaccorso, F.; Sun, Z.; Hassan, T.; Ferrari, A. C. Graphene Photonics and Optoelectronics. *Nat. Photonics* **2010**, *4*, 611–622.

16 Novoselov, K. S.; Geim, A. K.; Morozov, S. V.; Jiang, D.; Katsnelson, M. I.; Grigorieva, I. V.; Dubonos, S. V.; Firson, A. A. Two Dimensional Gas of Massless Dirac Fermions in Graphene. *Nature* **2005**, *438*, 197–200.

17 Saito, R.; Fujita, M.; Dresselhaus, M.; Dresselhaus, M. S. Electronic Structure of Chiral Graphene Tubules. *Appl. Phys. Lett.* **1992**, *60*, 2204–2206.

18 White, C. T.; Mintmire, J. W. Density of States Reflects Diameter in Nanotubes. *Nature* **1998**, *394*, 29–30.

19 McEuen, P. L. Nanotechnology: Carbon Based Electronics. *Nature* **1998**, *393*, 15–17.

20 McEuen, P. L.; Fuhrer, M. S.; Park, H. Single-Walled Carbon Nanotube Electronics. *IEEE Trans. Nanotechnol.* **2002**, *1*, 78–85.

21 Ohl, R. S. Light Sensitive Electric Device. United States Patent 2,402,662, 1941.

22 Sze, S. M. *Physics of Semiconductor Devices*, 2nd ed.; Wiley: London, 1981; Chapter 13.

23 Lee, J. U.; Gipp, P. P.; Heller, C. M. Carbon Nanotube p-n Junction Diodes. *Appl. Phys. Lett.* **2004**, *85*, 145–149.

24 Bosnick, K.; Gabor, N. M.; McEuen, P. L. Transport in Carbon Nanotube p-i-n Diodes. *Appl. Phys. Lett.* **2006**, *89*, No. 163121.

25 Huard, B.; Sulpizio, J. A.; Stander, N.; Todd, K.; Yang, B.; Goldhaber-Gordon, D. Transport Measurements Across a Tunable Potential Barrier in Graphene. *Phys. Rev. Lett.* **2007**, *98*, No. 236803.

26 Williams, J. R.; Dicarlo, L.; Marcus, C. M. Quantum Hall Effect in a Gate Controlled pn Junction of Graphene. *Science* **2007**, *317*, 638–641.

27 Ozyilmaz, B.; Jarillo-Herrero, P.; Efetov, D.; Abanin, D. A.; Levitov, L. S.; Kim, P. Electronic Transport and Quantum Hall Effect in Bipolar Graphene p-n-p Junctions. *Phys. Rev. Lett.* **2007**, *99*, No. 166804.

28 Gabor, N. M.; Song, J. C. W.; Ma, Q.; Nair, N. L.; Taychatanapat, T.; Watanabe, K.; Taniguchi, T.; Levitov, L. S.; Jarillo-Herrero, P. Hot Carrier-Assisted Intrinsic Photoresponse in Graphene. *Science* **2011**, *334*, 648–652.

29 Gabor, N. M.; Zhong, Z.; Bosnick, K.; Park, J.; McEuen, P. L. Extremely Efficient Multiple Electron-Hole Pair Generation in Carbon Nanotube Photodiodes. *Science* **2009**, *325*, 1367–1371.

30 Gabor, N. M. Extremely Efficient and Ultrafast: Electrons, Holes, and Their Interactions in the Carbon Nanotube PN Junction. Ph.D. Dissertation, Cornell University, Ithaca, NY, 2012; Chapter 3.

31 Bistritzer, R.; MacDonald, A. H. Electronic Cooling in Graphene. *Phys. Rev. Lett.* **2009**, *102*, No. 206410.

32 Winzer, T.; Knorr, A.; Malic, E. Carrier Multiplication in Graphene. *Nano Lett.* **2010**, *10*, 4839–4843.

33 Song, J. C.; Rudner, M. S.; Marcus, C. M.; Levitov, L. S. Hot Carrier Transport and Photocurrent Response in Graphene. *Nano Lett.* **2011**, *11*, 4688–4692.

34 Charlier, J. C.; Eklund, P. C.; Zhu, J.; Ferrari, A. C. Electron and phonon properties of graphene: their relationship with carbon nanotubes. In *Carbon Nanotubes: Advanced Topics in the Synthesis, Structure, Properties and Applications*; Jorio, A., Dresselhaus, G., Dresselhaus, M. S., Eds.; Topics in Applied Physics, Vol. 111; Springer-Verlag: New York, 2008; pp 673−709.

35 Kim, R.; Perebeinos, V.; Avouris, P. Relaxation of Optically Excited Carriers in Graphene. *Phys. Rev. B.* **2011**, *84*, No. 075449.

36 Winzer, T.; Malic, E. Impact of Auger Processes on Carrier Dynamics in Graphene. *ArXiv* **2012No. 1204.5650v1.**

37 Strait, J. H.; Wang, H.; Shivaraman, S.; Shields, V.; Spencer, M.; Rana, F. Very Slow Cooling Dynamics of Photoexcited Carriers in Graphene Observed by Optical-Pump Terahertz-Probe Spectroscopy. *Nano Lett.* **2011**, *11*, 4902–4906.

38 Xu, X.; Gabor, N. M.; Alden, J.; van der Zande, A.; McEuen, P. L. Photo-Thermoelectric Effect at a Graphene Interface Junction. *Nano Lett.* **2010**, *10*, 562–566.

39 Ashcroft, N. W.; Mermin, N. D. *Solid State Physics*; Thomson Learning: New York, 1976; p 256.

40 Peacock, A.; Verhoeve, P.; Rando, N.; van Dordrecht, A.; Taylor, B. G.; Erd, C.; Perryman, M. A. C.; Venn, R.; Howlett, J.; Goldie, D. J.; Lumley, J.; Wallis, M. Single Optical Photon Detection with a Superconducting Tunnel Junction. *Nature* **1996**, *381*, 135–137.

41 Kane, C. L.; Mele, E. J. Ratio Problem in Single Carbon Nanotube Fluorescence Spectroscopy. *Phys. Rev. Lett.* **2003**, *90*, No. 207401.

42 Perebeinos, V.; Avouris, P. Impact Excitation by Hot Carriers in Carbon Nanotubes. *Phys. Rev. B* **2006**, *74*, No. 121410 (R).

43 Wang, F.; Dukovic, G.; Brus, L. E.; Heinz, T. F. The Optical Resonances in Carbon Nanotubes Arise from Excitons. *Science* **2005**, *308*, 838–841.

44 Konabe, S.; Okada, S. Multiple Exciton Generation from a Single Photon in Single-Walled Carbon Nanotubes. *Phys. Rev. Lett.* **2012**, *108*, No. 227401.

45 Baer, R.; Rabani, E. Can Impact Excitation Explain Efficient Carrier Multiplication in Carbon Nanotube Photodiodes? *Nano Lett.* **2010**, *10*, 3277–3282.

46 Prechtel, L.; Song, L.; Manus, S.; Schuh, D.; Wegscheider, W.; Holleitner, A. W. Time-Resolved Picosecond Photocurrents in Contacted Carbon Nanotubes. *Nano Lett.* **2011**, *11*, 269–272.

47 Gabor, N. M.; Zhong, Z.; Bosnick, K.; McEuen, P. L. Ultrafast Photocurrent Measurement of the Escape Time of Electrons and Holes from Carbon Nanotube p-i-n Photodiodes. *Phys. Rev. Lett.* **2012**, *108*, No. 087404.

48 Misewich, J. A.; Martel, R.; Avouris, P.; Tsang, J. C.; Heinze, S.; Tersoff, J. Electrically Induced Optical Emission from a Carbon Nanotube FET. *Science* **2003**, *300*, 783–786.

49 Chen, J.; Perebeinos, V.; Freitag, M.; Tsang, J.; Fu, Q.; Liu, J.; Avouris, P. Bright Infrared Emission from Electrically Induced Excitons in Carbon Nanotubes. *Science* **2005**, *310*, 1171–1174.

50 Marty, L.; Adam, E.; Albert, L.; Doyon, R.; Menard, D.; Martel, R. Exciton Formation and Annihilation During 1D Impact Excitation of Carbon Nanotubes. *Phys. Rev. Lett.* **2006**, *96*, No. 136803.

51 Liao, A.; Zhao, Y.; Pop, E. Avalanche-Induced Current Enhancement in Semiconducting Carbon Nanotubes. *Phys. Rev. Lett.* **2008**, *101*, No. 256804.

52 Ueda, A.; Matsuda, K.; Tayagaki, T.; Kanemitsu, Y. Carrier Multiplication in Carbon Nanotubes Studied by Femtosecond Pump-Probe Spectroscopy. *Appl. Phys. Lett.* **2008**, *92*, No. 233105.

53 Wang, S.; Khafizov, M.; Tu, X.; Zheng, M.; Krauss, T. D. Multiple Exciton Generation in Single-Walled Carbon Nanotubes. *Nano Lett.* **2010**, *10*, 2381–2386.